COMPDYN 2009
ECCOMAS Thematic Conference on
Computational Methods in Structural Dynamics and Earthquake Engineering
M. Papadrakakis, N.D. Lagaros, M. Fragiadakis (eds.)
Rhodes, Greece, 22-24 June 2009

A GEOMETRIC MULTIGRID PRECONDITIONER FOR SOLVING TIME-HARMONIC ELASTODYNAMICS ON UNBOUNDED DOMAINS WITH PERFECTLY MATCHED LAYERS

Tsuyoshi Koyama[1] **and Sanjay Govindjee**[2]

[1]University of California, Berkeley
Department of Civil and Environmental Engineering
507 Davis Hall, Berkeley, CA 94720-1710
e-mail: tkoyama@berkeley.edu

[2]University of California, Berkeley
Department of Civil and Environmental Engineering
709 Davis Hall, Berkeley, CA 94720-1710
e-mail: s_g@berkeley.edu

Keywords: Perfectly Matched Layers, Multigrid, Preconditioner, Time-harmonic elastodynamics.

Abstract. *A scalable geometric multigrid preconditioner applicable to solving large-scale time-harmonic elastodynamic systems on unbounded domains modeled by Perfectly Matched Layers (PMLs) is presented. To solve for the forced motion of the elastodynamic system under time-harmonic excitation, one must solve a linear system of equations where the coefficient matrix is the stiffness matrix shifted by the mass matrix. Application of PMLs to model the radiation boundary condition renders these mass and stiffness matrices complex-valued symmetric and large-scale for accurate solutions. Large-scale matrices require the use of iterative methods to solve the linear systems for tractable solution time and computational memory. Complex-valued symmetric linear systems can be in general extremely difficult to solve iteratively, due to the lack of standard efficient techniques. To solve this linear system, a geometric multigrid preconditioner which can be combined with iterative methods such as GMRES is developed. The prolongation operator is constructed geometrically by constructing a nested hierarchy of meshes within superblocks and evaluating fine grid nodes with coarse grid shape functions. The smoothing operator is chosen as a Chebyshev smoother or Gauss-Seidel smoother. For a desired accuracy, to obtain satisfactory convergence rates we observe a mild restriction on the selectable PML component parameters. Heuristics for selecting PML parameters given a desired error in approximating the radiation boundary condition are presented to complement this solvability requirement our method poses on the range of selectable PML parameters. Under these restrictions, we see superior convergence of the method. A microelectromechanical disk resonator device is used to display the effectiveness of our method.*

1 Introduction

In many applications involving elastodynamics, one is interested in the behavior of a superstructure situated on top of a semi-infinite half domain, e.g., in earthquake engineering the behavior of a building atop soil. The motion of the superstructure couples with the underlying substrate giving rise to a source of energy dissipation in the form of outgoing propagating waves emanating from the superstructure. Proper modeling of this energy dissipation mechanism can be crucial in areas such as soil-structure interaction analysis, simulation of earthquake ground motions [1], and MEMS design [2].

To numerically model the energy dissipation mechanism arising from wave propagation into a semi-infinite half domain numerically on a finite computational domain, one must apply proper radiation boundary conditions. Among the many existing techniques modeling the radiation boundary condition [3], we select the technology of Perfectly Matched Layers [4] (PMLs) for its simplicity in application, sparsity in the resulting discretized matrices, and ability to absorb all outgoing waves with zero impedance mismatch at the domain boundaries in the continuous case. The application of PMLs mainly requires the selection of two parameters: the thickness of the PML and the absorbing function. These two parameters along with the method of discretization define how accurately the PML can approximate the radiation boundary condition. An optimal selection of the two components for a desired degree of accuracy is non-trivial. This difficulty or non-triviality is often noted but the numerical difficulty that can occur with respect to selection of these components is rarely mentioned.

To solve for the forced motion of the elastodynamic system under time-harmonic excitation, one must solve the linear system of equations,

$$\left(\mathbf{K} - \omega^2 \mathbf{M}\right) \mathbf{u} = \mathbf{F} \ . \tag{1}$$

Here $\mathbf{M}$, $\mathbf{K}$ are the mass and stiffness matrices of the numerically discretized system, $\mathbf{u}$ is the nodal displacement vector, $\mathbf{F}$ is the forcing vector, and ω is the forcing frequency. The computation of transfer functions as well as computation of eigenvalues of the elastodynamic system involve the solution of this linear system. It must be emphasized that the application of PMLs alters the structure of the matrices $\mathbf{M}$ and $\mathbf{K}$ from real-symmetric positive definite (SPD) to complex-valued symmetric (non-Hermitian), with the selection of the PML parameters affecting the degree to which they diverge from SPD. In the solution of small-scale problems, robust direct methods can be selected to solve the linear system. In the solution of large-scale problems, for tractable solution time and computational memory, one must resort to iterative methods which are highly sensitive to the matrix structure of the linear system. Since the selection of the PML parameters strongly alters the matrix structure, one must jointly consider the selection of PML parameters and solution procedure in this case. The complex-valued symmetric (non-Hermitian) property poses great difficulty in solvability due to the lack of standard tractable iterative solver techniques such that it may not be possible to select the PML parameters independent of the available solution method. Thus, a good understanding of the non-trivial relationship between PML parameters and accuracy is indispensable to select PML parameters that yield sufficient accuracy within the given restrictions.

To solve the complex-valued symmetric linear system, we employ a scalable geometric multigrid preconditioner combined with the iterative method GMRES. Multigrid (MG) has been selected as a preconditioner due to its success in solving large-scale linear systems arising from quasi-static elasticity [5]. Geometric Multigrid (GMG), the geometric variant, has been chosen due to the lack of a theoretical basis for generating an algebraic version for complex-valued

symmetric systems (theory exists only for the real symmetric positive definite [6, 7, 8] and some special indefinite cases [9, 10, 11]) as well as for its effectiveness when one has geometric information of the domain underlying the linear system of equations. In the GMG, the prolongation operator is constructed geometrically by constructing a nested hierarchy of meshes within superblocks and evaluating fine grid nodes with coarse grid shape functions for high scalability. The smoothing operator is chosen as the Gauss-Seidel or Chebyshev smoother.

An outline of the rest of the paper is as follows. Section 2 introduces the technology of Perfectly Matched Layers. A 1D scalar wave problem is used to develop heuristics for selection of PML parameters given a desired accuracy in approximating the radiation boundary conditions for a finite element discretized problem. In Section 3, the GMG preconditioned iterative linear solver is presented in combination with some mild restrictions on the selectable PML parameters for a convergent method. Section 4 presents numerical results to illustrates the applicability and scalability of the proposed method to large-scale 3D elastodynamic problems through a simulation of a MEMS disk resonator. The algorithm is implemented through a combination of *HiQLab* [12] the parallel numerical library *PETSc* [13] and run on a parallel processor machine.

2 Perfectly Matched Layers

In contrast to the coarse qualitative heuristics of [14, 15, 16], we present quantitative heuristics for PML parameter selection; the work is an extension of [17]. These heuristics are motivated through a 1D scalar wave problem, in which the sources of error of PMLs in modeling the radiation boundary condition for the finite element discretized problem are identified. (Though we restrict the presentation here to linear finite elements and a linear absorbing function $\lambda(x)$, heuristics can be constructed for higher-order elements as well as other profiles of $\lambda(x)$.)

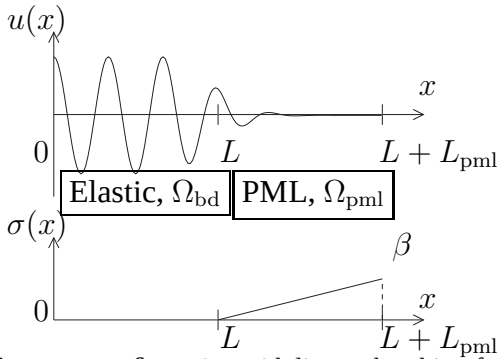

Figure 1: 1D scalar wave configuration with linear absorbing function profile.

2.1 1D scalar wave equation

Consider the 1D scalar wave equation with the application of PMLs as depicted in Fig. 1. The entire computational domain $[0, L + L_{\text{pml}}]$ is defined as the union of the bounded elastic domain $\Omega_{\text{bd}} := [0, L]$ and the wave absorbing PML domain $\Omega_{\text{pml}} := [L, L + L_{\text{pml}}]$. The governing equations for the system under time-harmonic assumptions for the displacement, $u(x,t) = \hat{u}(x)\exp(i\omega t)$, take the form of the Helmholtz equation,

$$\frac{d^2\hat{u}}{d\tilde{x}^2} + k^2\hat{u} = 0, \quad x \in [0, L + L_{\text{pml}}], \tag{2}$$

$$\tilde{x} = \int_0^x \lambda(s)ds, \quad \lambda(s) = 1 - \sigma(s)i, \tag{3}$$

where, ω is the forcing frequency, c is the wave speed, $k := \omega/c$ is the wave number, x is the original and $\tilde{x}$ the complex-stretched coordinate, and $i = \sqrt{-1}$. The absorbing function $\lambda(x)$, which determines the wave absorbing behavior of the PML, is selected as a linear profile with its imaginary part $\sigma(s)$ taking an end value of β in the PML domain. Harmonic excitation is applied at $x = 0$, yielding solutions to this equation consisting of two components, a right propagating (outgoing) wave of magnitude c_{out} and a left propagating (incoming) wave of magnitude c_{in}. Due to the application of PMLs, the waves propagating within the PML domain are exponentially damped.

2.2 End termination reflection

To mimic the radiation boundary condition, one desires $c_{\text{in}} = 0$, such that only outgoing waves are permitted as solutions. Thus the ratio [17],

$$r_{\text{end}} \quad := \quad \left| \frac{c_{\text{in}}}{c_{\text{out}}} \right| = \exp\left(-k\beta L_{\text{pml}}\right) \ , \tag{4}$$

can be considered a normalized measure of the quality of the boundary condition. This quantity will be given the name "end termination reflection", since it is due to the wave reflection arising from a finite end termination of the PML. This equation can be rewritten in the form,

$$-\frac{1}{2\pi}\log(r_{\text{end}}) \quad = \quad \beta\, n_{\text{wpml}} \ , \tag{5}$$

by defining the wave length $\lambda := 2\pi/k$ and the number of wave lengths in the PML $n_{\text{wpml}} := L_{\text{pml}}/\lambda$. r_{end} tends to zero as n_{wpml}, a non-dimensional measure of the length of the PML L_{pml}, and β, a non-dimensional measure of the strength of the absorbing function, increase. Additionally, one observes that the contours of constant r_{end} represent hyperbolas with respect to β and n_{wpml}. (β, n_{wpml}) are the two PML parameters one must properly select.

2.3 Interface reflection

Compared to the continuous problem where r_{end} is the only source of error, numerical discretization of the PML introduces another source. This error depends on many features of the PML such as node-spacing, finite element interpolation order, and PML absorbing function profile making the derivation of an analytical expression difficult. But, its character can be revealed by computing the reflection $r_{\text{computed}} = |c_{\text{in}}|/|c_{\text{out}}|$ from a finite element discretization of the 1D scalar wave problem introduced in the previous section. r_{computed} is obtained through dispersion analysis for equations with non-constant coefficients [17, 18, 19]. For simplicity, we assume the distance between nodes as constant.

In Fig. 2, the contours of constant computed reflection r_{computed} with respect to varying β and n_{wpml} is shown for a mesh discretization of $n_{\text{npw}} = 48$, where n_{npw} is the number of nodes per wave. The important detail to note is the shape of the curves of constant r_{computed} consist of a hyperbola plus a straight line emanating from the origin. The hyperbolas arise from the contribution r_{end} of Eqn. (5) and the straight lines are due to the discretization error. This contribution has been assigned the name "interface reflection" $r_{\text{interface}}$ [17]. Through numerical experimentation with various absorbing function profiles, we have observed that the shape of the contour curves representing the contribution $r_{\text{interface}}$ is identical to the function profile of $\sigma(s)$ (in Fig. 2 one has a linear profile and hence a straight line). This allows one to model the curves (in this case a straight line) as,

$$\beta \quad = \quad c(r_{\text{interface}}, n_{\text{npw}})\, n_{\text{wpml}} \ , \tag{6}$$

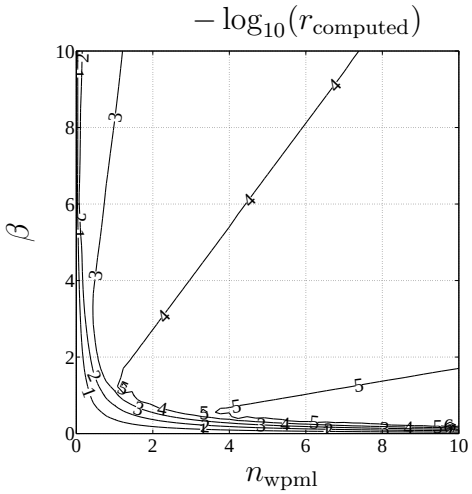

Figure 2: Computed reflection $-\log_{10}(r_{\text{computed}})$ for discretization $n_{\text{npw}} = 48$ with linear finite elements and linear absorbing function profile.

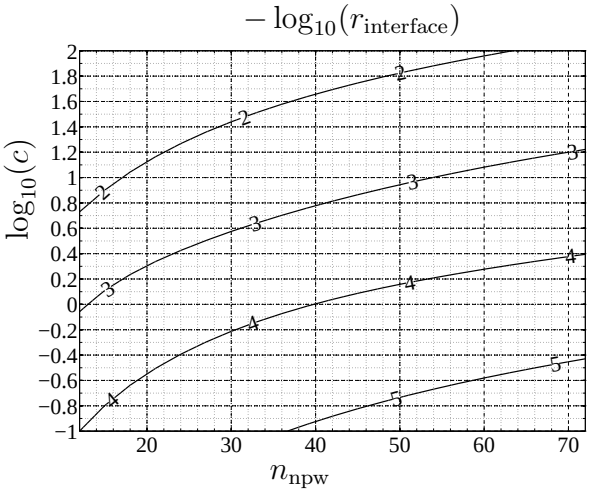

Figure 3: Interface reflection $-\log_{10}(r_{\text{interface}})$ with linear finite elements and linear absorbing function profile.

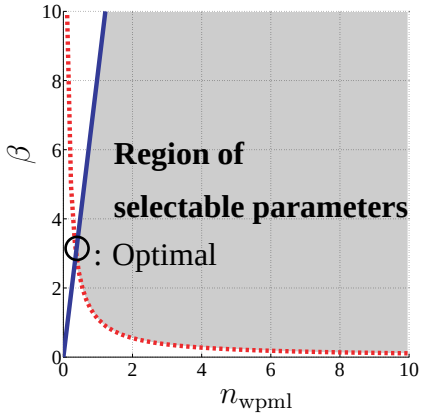

Figure 4: Reconstructed contour line for $-\log_{10}(r_{\text{tol}}) = 3$ for discretization $n_{\text{npw}} = 48$ with linear finite elements and linear absorbing function profile.

where the coefficient c is a function of $r_{\text{interface}}$ and n_{npw}. (In general c will also depend on the order of finite element interpolation and PML absorbing function profile. [20]) In Fig. 3 the relationship between c, n_{npw}, and $r_{\text{interface}}$ obtained numerically is presented, where the contours of constant $r_{\text{interface}}$ with respect to varying n_{npw} and c are plotted.

2.4 PML parameter selection

Given a desired tolerance of error r_{tol} and discretization n_{npw}, one can obtain a range of PML parameters (β, n_{wpml}) based on Eqns. (5,6) that satisfy this tolerance.

The case for $(r_{\text{tol}}, n_{\text{npw}}) = (10^{-3}, 48)$ is shown in Fig. 4. The dotted line corresponds to the curve obtained from setting $r_{\text{end}} = r_{\text{tol}}$ in Eqn. (5) and the solid line corresponds to the curve obtained from setting $r_{\text{interface}} = r_{\text{tol}}$ in Eqn. (6). As a result, the gray region defines the range of selectable PML parameters (β, n_{wpml}) for an error of 10^{-3}. One can see that we have been able to reconstruct what is observed in Fig. 2. Since n_{wpml} directly translates to the number of nodes and hence solution time, a minimal value is optimal. The obtained range of PML parameters implies that there exists an optimally small n_{wpml} and corresponding β

Though the parameter selection procedure that is presented here has been developed for the 1D scalar wave equation, it can be applied to multi-D scalar wave equations and vector-valued wave equations by only considering the component of the wave vector orthogonal to the Elastic/PML domain interface and then treating the problem as a 1D scalar wave problem.

3 Geometric Multigrid Preconditioner

To iteratively solve the linear system defined in Eqn. (1) for large-scale problems, a Geometric Multigrid (GMG) preconditioner is employed in combination with the GMRES iterative solver. GMG, the geometric variant of multigrid, has been chosen for its effectiveness and scalability in solving large-scale linear systems arising from quasi-static elasticity when one has geometric information of the physical system. It is also straightforward to extend to complex-symmetric systems. Special care though must be taken in selecting the two major components of MG, the prolongation operator and the smoother, since MG has been originally designed for SPD equations. Through investigation of the two grid convergence factor, it is shown that some mild restrictions exist on the selectable PML parameters for an effective GMG preconditioner.

3.1 Smoother

The smoothing operator is chosen as a Gauss-Seidel or a Chebyshev smoother. Since the coefficient matrix $(\mathbf{K} - \omega^2\mathbf{M})$ is complex-symmetric in the PML case, the application of these smoothers is not as straight-forward as the SPD case. Unconditionally convergent stationary methods such as row projections [5] as well as Krylov smoothers [21] can also be employed but due to either slow or varying convergence properties they are not selected here.

Gauss-Seidel The Gauss-Seidel smoother is only proven to be a convergent smoother for diagonally dominant or real-symmetric positive definite linear systems [22], which the coefficient matrix in our case is not. Still, Gauss-Seidel can be shown to be an effective smoother even for the complex-symmetric PML case under a restriction on the selectable PML parameters. Through Local Fourier Analysis (LFA) [5] one can show that for 2D and 3D elastodynamics with a linear PML absorbing function profile, Gauss-Seidel is convergent for $0 \leq \beta \lesssim 1$. This is one restriction the solution method puts on the selectable PML parameters. It must be emphasized that this restriction is one that any iterative method should encounter, since the upper

bound $\beta \lesssim 1$ stems from a loss of ellipticity of the material within the PML. This can be easily explained through a 2D scalar wave equation on a Cartesian grid with PML applied to absorb waves propagating in the x direction (the elastodynamic case can be shown in a similar manner). Locally, one can assume that the absorbing function defining the wave absorbing behavior is constant, $\lambda := 1 - \beta\, i$, with $0 \leq \beta < \infty$. By defining $\beta := \tan\alpha \;\; (0 \leq \alpha < \pi/2)$, one has $\lambda = \frac{1}{\cos\alpha} e^{-i\alpha}$ and thus obtains the following 2D Helmholtz equation in an anisotropic medium,

$$(\cos^2\alpha\; e^{2\alpha i})\frac{d^2\hat{u}}{dx^2} + \frac{d^2\hat{u}}{dy^2} + k^2\;\hat{u} = 0. \tag{7}$$

For any value of $\alpha > \pi/4$ ($\beta > 1$), the real part of the coefficient in front of the x derivative becomes negative; for $\beta > 1$, the PML behaves as an anisotropic viscoelastic material with negative stiffness in the x direction. This unstable behavior is not ideal and can cause problems for iterative methods due to introduction of small eigenvalues.

Chebyshev Chebyshev smoothers [23] are attractive for their efficiency in parallelization since they only involve matrix-vector operations. For the smoother to be effective, the eigenvalues of the operator $(\mathbf{K} - \omega^2\mathbf{M})$ must be contained in an ellipse of convergence defined by the selection of parameters in the Chebyshev polynomial. In the case of a complex-symmetric operator, a bounding box for the eigenvalues can be obtained to properly select the Chebyshev polynomial parameters so that the eigenvalues are contained within the ellipse [19]. This smoother loses its effectiveness as $\beta > 1$ for exactly the same reason the Gauss-Seidel smoother loses its effectiveness, but the performance degradation is not as extreme.

3.2 Prolongation operator

The different levels in the MG scheme are constructed automatically by parameterizing the block-generated mesh by a few length scale variables such as the approximate distance between adjacent nodes. The prolongation operator $\mathbf{P}$ from the coarse grid $\mathcal{G}_{\text{coarse}}$ to fine grid $\mathcal{G}_{\text{fine}}$ is constructed by the evaluation of fine grid nodes at the coarse grid shape functions. Let us denote the coarse grid nodes as $\mathbf{x}_i^c$ and the fine grid nodes as $\mathbf{x}_i^f$. Using the finite element shape functions on the coarse grid $N_j^c(\mathbf{x})$, the field on the coarse grid is represented as,

$$u(\mathbf{x}) \;\; = \;\; \sum_{j \in \mathcal{G}_{\text{coarse}}} N_j^c(\mathbf{x}) u_j^c \,. \tag{8}$$

Using the coarse grid values u_j^c, one can obtain an approximation of the nodal values on the fine grid u_i^f, by the interpolated values from the coarse grid shape functions [24],

$$u_i^f \;\; := \;\; u(\mathbf{x}_i^f) = \sum_{j \in \mathcal{G}_{\text{coarse}}} N_j^c(\mathbf{x}_i^f) u_j^c \,. \tag{9}$$

This is a linear mapping from the coarse grid values u_j^c to the fine grid values u_i^f, which is defined as the prolongation operator,

$$\mathbf{u}^f \;\; = \;\; \mathbf{P}\mathbf{u}^c \,, \tag{10}$$

whose components are,

$$P_{ij} \;\; = \;\; N_j^c(\mathbf{x}_i^f), \quad i \in \mathcal{G}_{\text{fine}}, \;\; j \in \mathcal{G}_{\text{coarse}}. \tag{11}$$

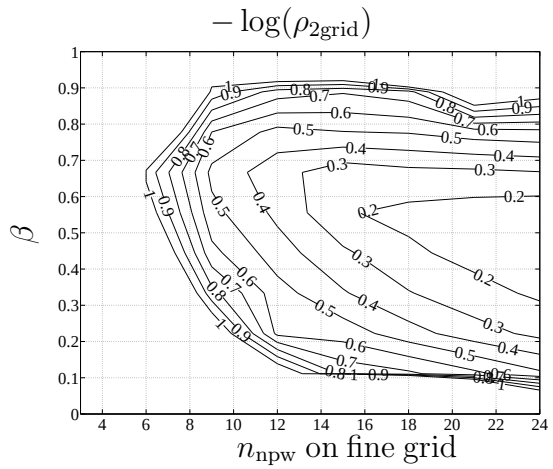

Figure 5: 2D elastodynamics: Two grid convergence factor $\rho_{2\text{grid}}$ for bilinear finite elements and linear absorbing function profile with Gauss-Seidel Smoother.

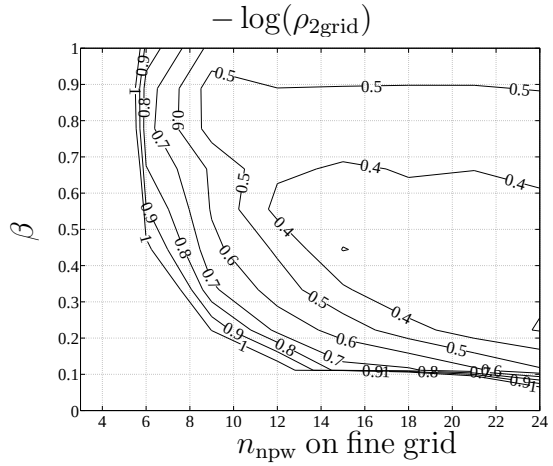

Figure 6: 2D elastodynamics: Two grid convergence factor $\rho_{2\text{grid}}$ for bilinear finite elements and linear absorbing function profile with Chebyshev smoother (polynomial order=2).

For the vector-valued case, each field is interpolated separately by the method introduced above. Since the finite element nodal shape functions have small support and little overlap, the prolongation operator is sparse. The block-generation based mesh construction strategy allows one to construct a data structure that allows a look up procedure for fast construction of the prolongation operators.

3.3 Two grid convergence factors

One can compute the two grid convergence factor, $\rho_{2\text{grid}}$, of the MG, a measure of the reduction in the error in one iteration of MG, to investigate what factors affect the performance of the proposed MG scheme. $\rho_{2\text{grid}}$ is computed for a sample 2D elastodynamic half space configuration to display the properties of the proposed method. The computational domain is truncated with the application of PMLs, and forced at a point on the free surface at a frequency which excites shear waves with wave discretization of n_{npw} points-per-wave. The fine grid has a discretization of n_{npw} and the coarse grid has half this value. The computed contours of constant $\rho_{2\text{grid}}$ for varying (n_{npw},β) using bilinear finite elements and a linear absorbing function profile are shown in Figs. 5 and 6 for the Gauss-Seidel and Chebyshev smoothers. $\rho_{2\text{grid}} < 1$ is required for convergence. The divergent behavior for $\beta \gtrsim 0.9$ using the Gauss-Seidel smoother is due to the divergence of the smoother, as mentioned earlier. It is clear that the Chebyshev

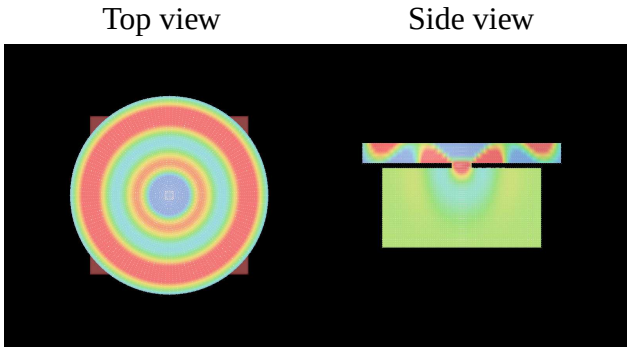

Figure 7: The 2nd radial contour mode shape of the 10 μm radius disk resonator; Color represents z displacement (Red: Positive, Blue: Negative).

smoother has a less stringent requirement for convergence on the selectable β parameter. The divergent behavior for $\beta \lesssim 0.1$ and $n_{\mathrm{npw}} \lesssim 7$ is due to a nonzero shift ω which prohibits a very coarse coarsest grid [10] and causes eigenvalues to cross the Imaginary axis of the complex plane [21]. The study of the two grid convergence factor imposes two constraints: $0 \leq \beta \lesssim 1$ and $n_{\mathrm{npw}} \gtrsim 5$ on the coarsest grid for convergent behavior of the iterative method.

4 Numerical example

To illustrate the effectiveness of the proposed method in solving a real 3D elastodynamic problem, the simulation of a MEMS disk resonator device is presented. The proposed method is implemented in the MEMS simulation software HiQLab [12] combined with the PETSc [13] library built on top of MPI, the linear solver MUMPS, the serial graph partitioner METIS, and conducted on a multiple processor machine. The cluster consists of 16 Linux compute nodes, each with two dual-core AMD Opteron 2216 processors for a total of 64 cores, connected via a Quadrics QsNet network.

A 20[μm] diameter polysilicon disk resonator is simulated and the forced motion at a radial contour mode of 716[MHz] is computed. Fig. 7 shows a 2D slice of the resonator through the center post and substrate, where the colors show the z direction displacements of the mode. One can see wave propagation through the substrate and the damping behavior in the PML region at the boundary of the computational domain, as well as parasitic z direction bending type motion in the disk.

Due to our current implementation of the code which uses the serial graph partitioner METIS, a computational constraint restricts the size of the problem we can compute, i.e., the discretization n_{npw} and the size of the PML n_{wpml}. This limits the 3D simulation to parameters $(\beta, n_{\mathrm{wpml}}) = (1, 6/13)$ and $n_{\mathrm{npw}} = 69.5$ on the finest grid in the MG hierarchy, which leads to a 6 million degrees-of-freedom (DOF) system. The hierarchy of levels constructed in the GMG preconditioner is shown in Table 1 with corresponding number of DOFs and discretization. For this simulation the Gauss-Seidel smoother has been employed. The selection of PML parameters yields an error of $-\log_{10}(r) = 1.26$, implying that the approximation of the radiation boundary condition should be accurate to at least the 1st digit. This accuracy can be investigated by computing the complex-valued eigenfrequency ω_0 closest to the forcing frequency ω and looking at its corresponding quality factor, $Q := \frac{\mathrm{Abs}(\omega_0)}{\mathrm{Imag}(\omega_0)}$. Q is a measure of the damping of the system vibrating in the mode corresponding to the eigenfrequency. Due to the computational constraints stated above, we cannot push the problem to full convergence in Q but see the value approaching 6000, which matches to the 1st digit the value of 6300 which we obtain from

Table 1: The 4 levels constructed for the geometric multigrid preconditioned GMRES iteration.

Level	Number of DOF	n_{npw}
1	49938	8.69
2	197574	17.4
3	977115	34.8
4	6140520	69.5

Table 2: GMRES iterations required to obtain a preconditioned relative residual of 1×10^{-10} (Parentheses denote the actual relative residual).

β	0	1.0	1.2
Iterations	38(5.0e-09)	41(3.3e-09)	160(2.0e-07)

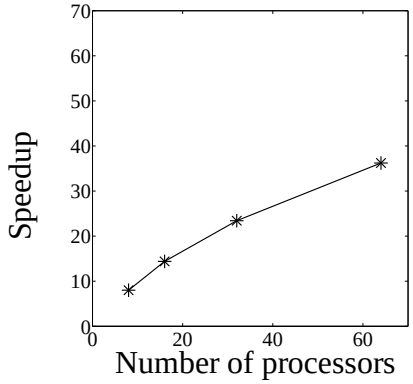

Figure 8: Strong scaling speedup with respect to number of processors for the solution of the disk resonator 6 million degrees-of-freedom problem.

a converged 2-D axisymmetric simulation. (The geometry of this disk allows an axissymetric analysis.)

The scalable behavior of the GMG preconditioned GMRES, can be see in Table 2 and Fig. 8. In Table 2 the number of iterations required to obtain a preconditioned relative residual of 1×10^{-10} for varying β is shown. As predicted, performance drops as $\beta > 1$, but for $0 \leq \beta \lesssim 1$ the number of iterations is fairly low. Fig. 8 shows the strong scaling speedup for the 6 million DOF problem.

5 Conclusions

A method to evaluate large-scale elastodynamic systems with PMLs based on a GMG preconditioned GMRES iterative solver has been presented. The GMG preconditioned GMRES poses restrictions on the selectable PML parameters ($0 \leq \beta \lesssim 1$) but one can expect similar restrictions on other iterative methods as well. To attain sufficient accuracy of the PML in modeling the radiation boundary conditions under this restriction, the relationship between PML parameters and accuracy along with heuristics for PML parameter selection have been presented. The numerical example of a MEMS disk resonator shows the scalable behavior of the proposed method to large-scale problems.

REFERENCES

[1] H. Bao, J. Bielak, O. Ghattas, L. Kallivokas, D. O'Hallaron, J. Shewchuck, J. Xu, Large-scale simulation of elastic wave propagation in heterogeneous media on parallel computers, Comput. Methods. Appl. Mech. Engrg. 152 (1998) 85–102.

[2] J. Wang, Z. Ren, C.-C. Nguyen, Self-Aligned 1.14-GHz Vibrating Radial-Mode Disk Resonators, in: Transducers'03, 2003, pp. 947–950.

[3] I. Harari, A survey of finite element methods for time-harmonic acoustics, Computer methods in applied mechanics and engineering 195 (2006) 1594–1607.

[4] U. Basu, A. Chopra, Perfectly matched layers for time-harmonic elastodynamics of unbounded domains: theory and finite-element implementation, Computer Methods in Applied Mechanics and Engineering 192 (2003) 1337–1375.

[5] U. Trottenberg, C. Oosterlee, A. Schueller, Multigrid, Academic Press, 2001.

[6] R. Falgout, An Introduction to Algebraic Multigrid, Computing in Science and Engineering 8 (6) (2006) 24–33.

[7] J. Mandel, M. Brezina, P. Vanek, Energy Optimization of Algebraic Multigrid Bases, Computing 62 (1999) 205–228.

[8] P. Vanek, M. Brezina, J. Mandel, Convergence of algebraic multigrid based on smoothed aggregation, Numerische Mathematik 88 (3) (2001) 559–579.

[9] R. Bank, A Comparison of Two Multilevel Iterative Methods for Nonsymmetric and Indefinite Elliptic Finite Element Equations, SIAM Journal of Numerical Analysis 18 (4) (1981) 724–743.

[10] J. Bramble, D. Kwak, J. Pasciak, Uniform Convergence of Multigrid V-Cycle Iterations for Indefinite and Nonsymmetric Problems, SIAM Journal of Numerical Analysis 31 (6) (1994) 1746–1763.

[11] Y. Shapira, Multigrid methods for 3-D definite and indefinite problems, Applied Numerical Mathematics 26 (1998) 377–398.

[12] D. Bindel, HiQLab, http://cims.nyu.edu/ dbindel/hiqlab/.

[13] S. Balay, K. Buschelman, W. D. Gropp, D. Kaushik, M. G. Knepley, L. C. McInnes, B. F. Smith, H. Zhang, PETSc Web page, http://www.mcs.anl.gov/petsc (2001).

[14] I. Harari, M. Slavutin, E. Turkel, Analytical and Numerical Studies of a Finite Element PML for the Helmholtz Equation, Journal of Computational Acoustics 8 (1) (2000) 121–137.

[15] E. Heikkola, T. Rossi, J. Toivanen, Fast direct solution of the Helmholtz equation with a perfectly matched layer or an absorbing boundary condition, International Journal for Numerical Methods in Engineering 57 (2003) 2007–2025.

[16] F. Collino, P. Monk, Optimizing the perfectly matched layer, Computer Methods in Applied Mechanics and Engineering 164 (1998) 157–171.

[17] D. Bindel, S. Govindjee, Elastic PMLs for resonator anchor loss simulation, International Journal for Numerical Methods in Engineering 64 (2005) 789–818.

[18] D. Bindel, Structured and Parameter-Dependent Eigensolvers for Simulation-Based Design of Resonant MEMS, Ph.D. thesis, University of California, Berkeley (2006).

[19] T. Koyama, Efficient Evaluation of Damping in Resonant MEMS, Ph.D. thesis, University of California, Berkeley (2008).

[20] T. Koyama, S. Govindjee, Optimal parameter selection of the Perfectly Matched Layer for applications in time harmonic wave propagation, Submitted.

[21] H. Elman, O. Ernst, D. O'Leary, A multigrid method enhanced by Krylov subspace iteration for discrete Helmholtz equations, SIAM Journal on Scientific Computing 23 (4) (2001) 1290–1314.

[22] G. Golub, C. van Loan, Matrix Computations, John Hopkins, 1983.

[23] M. Adams, M. Brezina, J. Hu, Parallel multigrid smoothing: polynomial versus Gauss-Seidel, Journal of Computational Physics 188 (2) (2003) 593–610.

[24] Y. Feng, D. Peric, D. Owen, A non-nested Galerkin multi-grid method for solving linear and nonlinear solid mechanics problems, Computer methods in applied mechanics and engineering 144 (1997) 307–325.